High-spin states in ^{188}Au: Further evidence for nonaxial shape

Y. D. Fang,[1] Y. H. Zhang,[1] M. Oshima,[2] Y. Toh,[2] F. R. Xu,[3] Y. Shi,[3] X. H. Zhou,[1] M. L. Liu,[1] Y. X. Guo,[1] M. Koizumi,[2] A. Kimura,[2] Y. Hatsukawa,[2] T. Morikawa,[4] M. Nakamura,[4] M. Sugaware,[5] and H. Kusakari[6]

[1]*Institute of Modern Physics, Chinese Academy of Sciences, Lanzhou, China*

[2]*Japan Atomic Energy Agency, Tokai, Ibaraki 319-1195, Japan*

[3]*Department of Technical Physics and MOE Key Laboratory, Peking University, Beijing 100871, People's Republic of China*

[4]*Department of Physcis, Kyushu University, Fukuoka 812-81, Japan*

[5]*Chiba Institute of Technology, Narashino, Chiba 275-0023, Japan*

[6]*Chiba University, Inage-ku, Chiba 263-8512, Japan*

(Received 5 July 2010; revised manuscript received 5 November 2010; published 6 December 2010)

The high-spin level structure of ^{188}Au has been investigated via the ^{173}Yb(^{19}F,4$n\gamma$) reaction at beam energies of 86 and 90 MeV. The previously reported level scheme has been modified and extended significantly. A new $I^{\pi} = 20^{+}$ state associated with $\pi h_{11/2}^{-1} \otimes \nu i_{13/2}^{-2} h_{9/2}^{-1}$ configuration and two new rotational bands, one of which is built on the $\pi h_{9/2} \otimes \nu i_{13/2}$ configuration, have been identified. The prolate-to-oblate shape transition through triaxial shape has been proposed to occur around ^{188}Au for the $\pi h_{9/2} \otimes \nu i_{13/2}$ bands in odd-odd Au isotopes. Evidence for $\pi h_{11/2}^{-1} \otimes \nu i_{13/2}^{-1}$ structure of nonaxial shape with $\gamma < -70^{\circ}$ has been obtained by comparison with total Routhian surface and cranked-shell-model calculations.

DOI: 10.1103/PhysRevC.82.064303 PACS number(s): 21.10.Re, 23.20.Lv, 27.70.+q

I. INTRODUCTION

There is a well-known region of shape coexistence in Pt-Au-Hg nuclei. The low-lying 0^{+}, 2^{+} states in the Hg isotopes are thought to have an oblate shape while the second 0^{+}, 2^{+} states decrease rapidly in excitation energy from ^{188}Hg to ^{184}Hg and have been described as having prolate shapes (see Ref. [1] and references therein). In contrast to the Hg isotopes, the lowest 0^{+} states in $^{178-186}$Pt are prolate with the excited states 0^{+} being oblate [2,3]. In Au isotopes a shape competition is well known between slightly deformed oblate shape in heavier isotopes and moderately deformed prolate shape in lighter isotopes [4–9]. The proton Fermi level in Au nuclei lies between the $\pi h_{11/2}$ and the $\pi h_{9/2}$ subshells. For nuclei with oblate shape the odd proton occupies a low-Ω $h_{11/2}$ orbital, while for prolate shape it occupies a low-Ω $h_{9/2}$ orbital. The $^{184-186}$Au ground states have been known to be prolately deformed [4–7], whereas the ^{187,189}Au ground states are associated with oblate configuration [8,9]. Therefore, the spectroscopic information of ^{188}Au is of particular interest as it lies at the critical point of prolate-to-oblate shape transition where the change in collective structure should be most drastic. One expects that a variety of shapes depending on the configurations of the excited quasiparticles could be observed experimentally in ^{188}Au.

Another interesting phenomenon is the so-called γ-soft nuclei in the $A \sim 190$ transitional region. Such γ-soft nuclei represent the best cases to study shape changes induced by the occupation of specific high-j orbitals near the Fermi surface. More recently, the nonaxiality of the nuclear shape has been suggested for the $^{190-193}$Au nuclei [10–13]. However, the nonaxial shapes in ^{188,189}Au are still unclear. To reveal details of the nature of these nonaxial nuclei, systematic and further experimental investigations are needed. ^{188}Au seems to be a good candidate for further studies so long as its location in the chart of nuclides is concerned.

Prior to this work, high-spin states in ^{188}Au were investigated by Janzen *et al.* [7] via ^{173}Yb (^{19}F,4$n\gamma$) reaction. The high-spin level structure has been proposed to be associated with $\pi h_{11/2}^{-1} \otimes \nu i_{13/2}^{-1}$ and $\pi h_{11/2}^{-1} \otimes \nu i_{13/2}^{-2} j$ [$j = (p_{3/2}, f_{5/2})$] oblate configurations [7]. The present work aims to study the shape coexistence phenomenon in ^{188}Au and addresses the shape evolution for the Au isotopes.

In this article, we report the experimental results on high-spin structure in ^{188}Au. Several level sequences have been identified for the first time and the previous level scheme has been largely modified. The interpretation of the observed structures has been made on the basis of total Routhian surface (TRS) and cranked-shell-model (CSM) calculations. The experimental details and the construction of the level scheme are described in Sec. II and the results are discussed in Sec. III. A brief summary is presented in Sec. IV.

II. EXPERIMENTS AND RESULTS

A. Measurements

The excited states of ^{188}Au were populated via the 4n evaporation channel following the fusion of a ^{19}F beam with an ^{173}Yb target. The ^{19}F beam was provided by the tandem accelerator at the Japan Atomic Energy Agency (JAEA). The target was a 2.2 mg/cm^2 thickness isotopically enriched ^{173}Yb metallic foil with a 7.0 mg/cm^2 Pb backing. A γ-ray detector array GEMINI [14] was used to measure the X-γ-t and γ-γ-t coincidence. Here t refers to the relative time difference between any two coincident γ rays detected within $\pm$100 ns. The array consists of 18 large-volume high-purity germanium (HPGe) detectors with bismuth germanate anti-Compton shields; 6 detectors had an efficiency of 40% each and the others had 70% relative to 3×3-in. NaI. The energy and efficiency calibrations were made using ^{60}Co, ^{133}Ba, and ^{152}Eu standard sources. Typical energy resolutions were about 2.0–2.5 keV at full width at half maximum for the 1332.5-keV line.

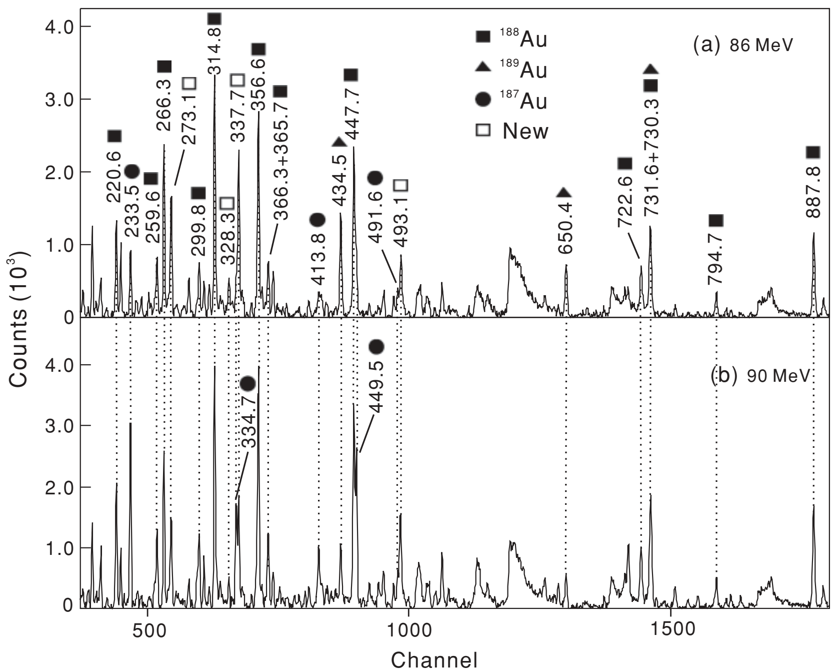

FIG. 1. Au K x-ray-gated spectra at 86-MeV (top panel) and 90-MeV (bottom panel) beam energies.

To identify the in-beam γ rays belonging to ^{188}Au, relative γ-ray yields were measured at beam energies of 86 and 90 MeV, respectively. At each beam energy, about 80×10^6 γ-γ coincidence events were accumulated and sorted online into a symmetric E_γ-E_γ matrix of $4k \times 4k$ size. The γ-ray spectra in this experiment were very complex; the photon peaks were often doublets or contaminated by the γ rays from other reaction channels. Along with the ^{188}Au nucleus, the ^{187,189}Au nuclei were also produced in a ^{173}Yb(^{19}F, $xn\gamma$) reaction. The level schemes of ^{187}Au and ^{189}Au had been well known from previous studies [8,9]. The Au K x-ray-gated spectra are displayed in Fig. 1. As can be seen in this figure, the relative yields of known γ rays from ^{189}Au (434.5- and 650.4-keV lines [9]) decrease apparently at the higher beam energy, while those from the ^{187}Au (233.5-, 334.7-, 413.8-, 449.5-, and 491.6-keV lines [8]) are much enhanced with increasing beam energy. The relative yields of the known γ rays (220.6-, 259.6-, 266.3-, 299.8-, 314.8-, 356.6-, 447.7-, 722.6-, and 887.8-keV lines [7]) from ^{188}Au were found to change smoothly as the beam energy increases from 86 to 90 MeV. The relative yields of the new 273.1-, 328.3-, 337.7-, and 493.1-keV γ rays have a similar trend with the known γ rays from ^{188}Au. We note that in a previous article [9], γ-ray excitation functions had been measured using reaction ^{174}Yb (^{19}F, $xn\gamma$) with beam energies of 86 through 100 MeV. Checking carefully the relative intensity of corresponding γ rays in Fig. 4 of Ref. [9], we found that the relative intensity of the 273-, 328-, and 338-keV γ rays have a similar pattern with the known γ rays from ^{188}Au as the beam energy increases from 86 MeV toward 100 MeV. This information suggests strongly that the new 273.1-, 328.3-, 337.7-, and 493.1-keV γ rays observed in this experiment could be assigned to ^{188}Au.

To obtain the multipolarity information of emitting γ rays, the detectors were divided into four groups. Two asymmetric coincidence matrices were constructed using the γ rays detected at all angles (y axis) against those observed at 47°, 147° and 90°, 105° (x axis), respectively. From these two matrices, the angular distribution asymmetry ratios, defined as $R_{\mathrm{ADO}}(\gamma) = I_\gamma(40^\circ)/I_\gamma(98^\circ)$, were extracted from the γ-ray intensities $I_\gamma(40^\circ)$ and $I_\gamma(98^\circ)$ in the coincidence spectra gated by γ transitions (on the y axis) of any multipolarity (it is supposed that the angular distribution effects of the gating γ transitions could be neglected in the asymmetric matrices). Usually, a single gate was used for strong peaks. For some weak transitions, the sum-gated spectra were used to get high statistics. In the present geometry, stretched quadrupole transitions were adopted if $R_{\mathrm{ADO}}(\gamma)$ values were larger than unity [an average value of $R_{\mathrm{ADO}}(\gamma) = 1.16 \pm 0.15$ was obtained for the known $E2$ transitions in ^{187,189}Au], and dipole transitions were assumed if $R_{\mathrm{ADO}}(\gamma)$'s were significantly less than 1.0.

B. Level scheme

The high-spin level scheme of ^{188}Au was established experimentally up to $I^\pi = 24^+$ by means of the heavy-ion ^{173}Yb(^{19}F,$4n\gamma$) reaction [7]. Detailed knowledge of low-spin states in ^{188}Au were provided from decay studies of ^{188}Hg [15].

In the present study, the level scheme of ^{188}Au has been extended considerably. As shown in Fig. 2, more than 40 new transitions have been placed in the present level scheme. Particularly, we have identified two new $\triangle I = 2$ bands for the first time. The γ-transition energies in the level scheme are within an uncertainty of 0.5 keV, and the ordering of the transitions in various bands are established on the basis of γ-γ coincidence relationships, γ-ray energy sums, and γ-ray relative intensities. The relative spins within a band are proposed in terms of the measured ADO ratios of emitting γ rays. The γ-ray energies, spin and parity assignments, relative γ-ray

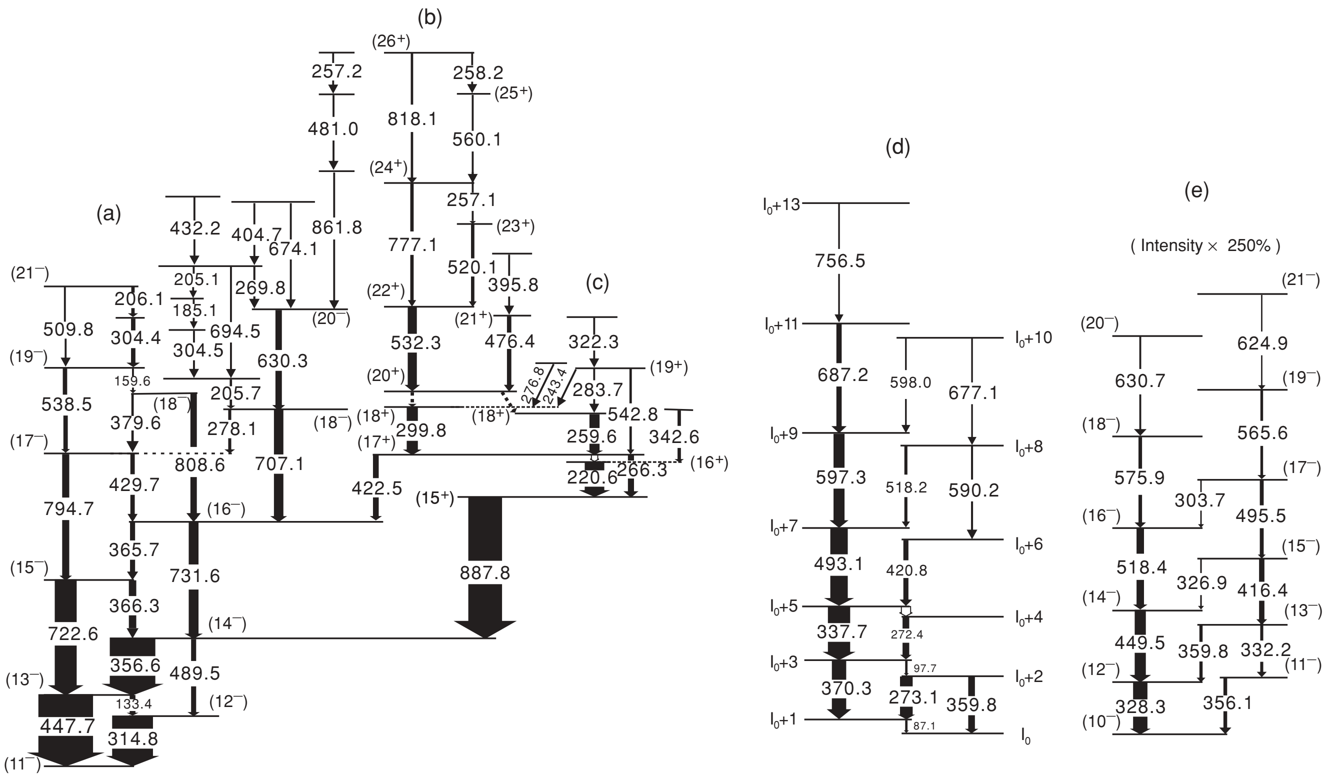

FIG. 2. Level scheme of ^{188}Au deduced from this work.

intensities, branching ratios, extracted $B(M1)/B(E2)$ values, and the R_{ADO} values are presented in Table I. It should be noted that the relative intensities for some uncontaminated γ rays could be measured in the total projection spectrum. Most of the values were extracted from the spectra gated on the bottom transitions in the band. Some brief explanations of the level scheme are given as follows.

Band (a) is most strongly populated in this experiment. This band was observed previously and suggested to be associated with an oblate $\pi h_{11/2}^{-1} \otimes \nu i_{13/2}^{-1}$ configuration [7]. A typical coincidence spectrum gated on the 447.7-keV transition is presented in Fig. 3(a), showing the quality of the data. For the levels above the (17^-) state, some modifications have been made in the present level scheme as compared to the previous work of Janzen *et al.* [7]. First, the previously reported 704.4-, 693.7-keV cascade, which was assigned to feed the (17^-) state, cannot be confirmed in our work. The coincidence relationships for the 704.4- and 693.7-keV transitions have been checked with care. No evidence has been found for the existence of 704.4-keV transition feeding the (17^-) state. A 694.5-keV transition is in strong coincidence with the 205.7- and 707.1-keV lines. This leads to the conclusion that the previously reported 704.4- and 693.7-keV transitions should originate from closely spaced lines having energies of 707.1- and 694.5-keV, respectively. Second, a new 379.6-keV γ ray is observed and assigned as the $(18^-)\rightarrow(17^-)$ transition in parallel with the 538.5- and 808.6-keV lines. One can see from Fig. 3(b) that this transition is in strong coincidence with the 159.6-, 429.7-, 794.7-, and 722.6-keV transitions but not with the 538.5- and 808.6-keV transitions. The R_{ADO} value for the 379.6 keV transition (Table I) suggests a $\lambda = 1$ transition. Finally, self-coincidence of the 794-keV transition [7] could not be confirmed in our data. Considering the level structure of band (a) in Fig. 2, we tend to classify the 509.8-, 538.5-, 794.7-, 722.6-, and 447.7-keV transitions as the unfavored signature of band (a) and the 808.6-, 731.6-, and 489.5-keV transitions as the favored signature of band (a). This classification is consistent with the level schemes in neighboring odd-odd ^{190,192}Au isotopes [12] taking into account the similar level spacings.

As for the positive-parity states, a new $I^\pi = 20^+$ level is identified which decays toward two (18^+) states via two low-energy transitions. This is supported by the observation of two new 243.4- and 276.8-keV transitions. As can be seen in Figs. 3(c) and 3(d), the 532.3-keV transition is in coincidence with the 299.8-, 259.6-, and 422.5-keV γ rays, while the 243.4- and 276.8-keV transitions have the same coincidence relationships with the 299.8- and 422.5-keV lines but not with the 259.6-keV line. This indicates that the (20^+) level deexcites toward two different (18^+) levels via two unobserved transitions. The energy limit for the γ-ray detector array GEMINI is about 50 keV. These two transitions were not observed experimentally owing to low detection efficiency and their highly converted nature. With the observation of the $I^\pi = 20^+$ state, we were able to identity two different structures: One is built on top of the $I^\pi = 20^+$ level and the other on top of the $I^\pi = 15^+$ state, corresponding to band (b) and structure (c), respectively. We note that similar structures built on the $I^\pi = 20^+$ state and $I^\pi = 15^+$ state have been found in odd-odd ^{190,192}Au isotopes [12].

TABLE I. γ-ray transition energies, spin and parity assignments, γ-ray intensities, branching ratios, extracted $B(M1)/B(E2)$ ratios, ADO ratios, and γ-ray multipolarities in ^{188}Au.

E_γ (keV)[a]	$J_i^\pi \rightarrow J_f^\pi$[b]	I_γ[c]	λ[d]	$B(M1)/B(E2)$[e]	R_{ADO}	ML
Band (a)						
314.8	$(12^-) \rightarrow (11^-)$	121(9)			0.83(7)	$M1/E2$
447.7	$(13^-) \rightarrow (11^-)$	162(13)			1.12(14)	$E2$
133.4	$(13^-) \rightarrow (12^-)$	17(2)	8.79(57)	0.61(7)	0.66(9)	$M1/E2$
489.5	$(14^-) \rightarrow (12^-)$	15(2)			1.24(23)	$E2$
356.6	$(14^-) \rightarrow (13^-)$	135(10)	0.12(01)	3.52(31)	0.89(7)	$M1/E2$
722.6	$(15^-) \rightarrow (13^-)$	65(5)			1.19(10)	$E2$
366.3	$(15^-) \rightarrow (14^-)$	22(3)	2.22(22)	1.26(13)	0.80(8)	$M1/E2$
731.6	$(16^-) \rightarrow (14^-)$	29(3)			1.08(11)	$E2$
365.7	$(16^-) \rightarrow (15^-)$	25(3)	1.16(12)	2.58(12)	0.79(7)	$M1/E2$
794.7	$(17^-) \rightarrow (15^-)$	21(3)			1.07(12)	$E2$
429.7	$(17^-) \rightarrow (16^-)$	13(3)	3.15(31)	0.88(9)	0.66(11)	$M1/E2$
808.6	$(18^-) \rightarrow (16^-)$	19(4)			1.26(28)	$E2$
538.5	$(19^-) \rightarrow (17^-)$	13(3)			1.29(18)	$E2$
379.6	$(18^-) \rightarrow (17^-)$	7(2)	2.56(60)	1.73(40)	0.94(17)	$M1/E2$
159.6	$(19^-) \rightarrow (18^-)$	4.0(9)	3.48(29)	2.25(19)	0.87(16)	$M1/E2$
304.4	$(20^-) \rightarrow (19^-)$	13(3)			0.87(13)	$M1/E2$
206.1	$(21^-) \rightarrow (20^-)$	10(2)			0.75(13)	$M1/E2$
509.8	$(21^-) \rightarrow (19^-)$	2.0(7)				
707.1	$(18^-) \rightarrow (16^-)$	28(5)			1.21(15)	$E2$
278.1	$(18^-) \rightarrow (17^-)$	9(2)	2.94(31)	1.96(21)	0.92(21)	$M1/E2$
630.3	$(20^-) \rightarrow (18^-)$	19(3)			1.25(27)	$E2$
861.8	$\rightarrow (20^-)$	5.0(8)				
269.8		5(1)			0.86(14)	$M1/E2$
432.2		4(1)			0.85(17)	$M1/E2$
185.1		2(1)				
257.2		4.0(9)				
481.0		4(2)				
404.7		4(1)			0.66(17)	$M1/E2$
674.1		3.0(4)				
304.5		4(1)			0.77(14)	$M1/E2$
694.5					1.24(24)	$E2$
Band (b)						
276.8	$\rightarrow (18^+)$	1.0(2)				
299.8	$(18^+) \rightarrow (17^+)$	33(3)			0.82(7)	$M1/E2$
532.3	$(22^+) \rightarrow (20^+)$	27(3)			1.26(13)	$E2$
476.4	$(21^+) \rightarrow (20^+)$	13(1)			0.96(12)	$M1/E2$
777.1	$(24^+) \rightarrow (22^+)$	10(2)			1.07(13)	$E2$
520.1	$(23^+) \rightarrow (22^+)$	10(1)			0.89(10)	$M1/E2$
818.1	$(26^+) \rightarrow (24^+)$	5(1)			1.41(27)	$E2$
560.1	$(25^+) \rightarrow (24^+)$	4(1)				
395.8	$\rightarrow (21^+)$	4(1)			0.70(11)	$M1/E2$
257.1	$(24^+) \rightarrow (23^+)$	2(1)				
258.7	$(26^+) \rightarrow (25^+)$	3(1)				
Structure (c)						
266.3	$(17^+) \rightarrow (15^+)$	20(2)			1.12(10)	$E2$
220.6	$(16^+) \rightarrow (15^+)$	58(5)			0.79(6)	$M1/E2$
259.6	$(18^+) \rightarrow (17^+)$	30(3)			0.94(8)	$M1/E2$
542.8	$(19^+) \rightarrow (17^+)$	5(1)				
243.4	$(19^+) \rightarrow (18^+)$	2(1)				
342.6	$(17^+) \rightarrow (16^+)$	10(1)			0.88(17)	$M1/E2$
283.7	$(19^+) \rightarrow (18^+)$	3(1)				
322.3		3(1)				
Band (d)						
87.1	$I_0 + 1 \rightarrow I_0$	>8(1)			0.89(15)	$M1/E2$
273.1	$I_0 + 2 \rightarrow I_0 + 1$	>37(3)	0.58(13)	0.36(8)	0.53(6)	$M1/E2$

TABLE I. (*Continued.*)

E_γ (keV)[a]	$J_i^\pi \to J_f^\pi$ [b]	I_γ [c]	λ[d]	$B(M1)/B(E2)$[e]	R_{ADO}	ML
359.8	$I_0+2 \to I_0$	>19(2)			1.11(11)	$E2$
370.3	$I_0+3 \to I_0+1$	>42(5)			1.30(12)	$E2$
97.7	$I_0+3 \to I_0+2$	>6(2)	7.01(65)	0.74(18)	0.68(17)	$M1/E2$
337.7	$I_0+5 \to I_0+3$	66(5)			1.17(13)	$E2$
272.4	$I_0+4 \to I_0+3$	19(3)			0.84(12)	$M1/E2$
420.8	$I_0+6 \to I_0+5$	15(2)			0.53(9)	$M1/E2$
493.1	$I_0+7 \to I_0+5$	52(6)			1.18(11)	$E2$
590.2	$I_0+8 \to I_0+6$	6(2)			1.06(30)	$E2$
518.2	$I_0+8 \to I_0+7$	9(2)			0.62(15)	$M1/E2$
597.3	$I_0+9 \to I_0+7$	33(4)			1.22(11)	$E2$
677.1	$I_0+10 \to I_0+8$	5(2)				
598.0	$I_0+10 \to I_0+9$	5(2)				
687.2	$I_0+11 \to I_0+9$	16(3)			1.17(27)	$E2$
756.5	$I_0+13 \to I_0+11$	5(2)			1.21(29)	$E2$
Band (e)						
356.1	$(11^-) \to (10^-)$	4(1)			0.48(6)	$M1/E2$
328.3	$(12^-) \to (10^-)$	17(2)			1.16(11)	$E2$
332.2	$(13^-) \to (11^-)$	4(1)			1.26(35)	$E2$
359.8	$(13^-) \to (12^-)$	4(1)			0.60(9)	$M1/E2$
449.5	$(14^-) \to (12^-)$	13(2)			1.26(16)	$E2$
416.4	$(15^-) \to (13^-)$	6(1)			1.39(29)	$E2$
326.9	$(15^-) \to (14^-)$	2(1)			0.36(7)	$M1/E2$
518.4	$(16^-) \to (14^-)$	9(2)			1.13(11)	$E2$
495.5	$(17^-) \to (15^-)$	5(1)			1.00(23)	$E2$
303.7	$(17^-) \to (16^-)$	1.0(3)				
575.9	$(18^-) \to (16^-)$	4(2)			1.17(16)	$E2$
565.6	$(19^-) \to (17^-)$	3(1)			1.09(19)	$E2$
630.7	$(20^-) \to (18^-)$	2(1)			1.37(51)	$E2$
624.6	$(21^-) \to (19^-)$	2(1)				
Transitions	from band (b) and structure (c)	*toband*(a)				
887.8	$(15^+) \to (14^-)$	100(8)			0.75(6)	$E1$
422.5	$(17^+) \to (16^-)$	17(2)			0.75(9)	$E1$

[a]Uncertainties between 0.1 and 0.5 keV.
[b]See text for details about the spin and parity assignments.
[c]Uncertainties between 5% and 30%. Normalized to the 887.8-keV transition.
[d]Branching ratio: $T_\gamma(I \to I-2)/T_\gamma(I \to I-1)$, $T_\gamma(I \to I-2)$ and $T_\gamma(I \to I-1)$ are the relative γ intensities of the $E2$ and $M1$ transitions depopulating the level I, respectively.
[e]Extracted from the branching ratios assuming $\delta^2 = 0$.

As discussed in Sec. II A, the 337.7-keV transition can be assigned to ^{188}Au by the excitation function measurements [9]. The γ-γ coincidence relationships have been analyzed with care for all the γ rays associated with the 337.7-keV transition, leading to the newly established band structure in Fig. 2 labeled as (d). Some representative coincidence spectra are given in Fig. 4. The 87.1- and 97.7-keV low-energy transitions are weak because of their highly converted nature and low detection efficiency. They can still be seen clearly in Fig. 4(d). Based on the measured ADO ratios, we have assigned an $M1/E2$ multipolarity for the 87.1- and 97.7-keV transitions and an $E2$ multipole order for the 359.8- and 370.3-keV lines.

The 272.8-keV line in Fig. 4(a) is in coincidence with all the γ rays in band (d) as well as itself [see Fig. 4(d)]. From careful analysis of the γ-γ coincidence spectra, we have identified the 272.8-keV line as a doublet, that is, a 272.4-keV transition deexciting the (I_0+4) level and an $(I_0+2) \to (I_0+1)$ 273.1-keV line in band (d) (see Fig. 2). This assignment is based on the following considerations.

(i) The ADO ratio for the 272.4- and 273.1-keV transitions has been analyzed using 370.1- and 337.7-keV transitions, respectively, as gates. A $\Delta I = 1$ dipole character has been determined for the 272.4- and 273.1-keV γ rays in each of the gated spectra. We present, in Fig. 5, the 492-keV gated spectra in which a cascade of $E2$ transitions from the $\pi 1/2^-[541]$ band of ^{187}Au are also presented for comparison; the top and bottom panels correspond to the projected spectrum at 40° and 98°, respectively. One can see clearly that the 272.8-keV line is definitely a dipole transition.

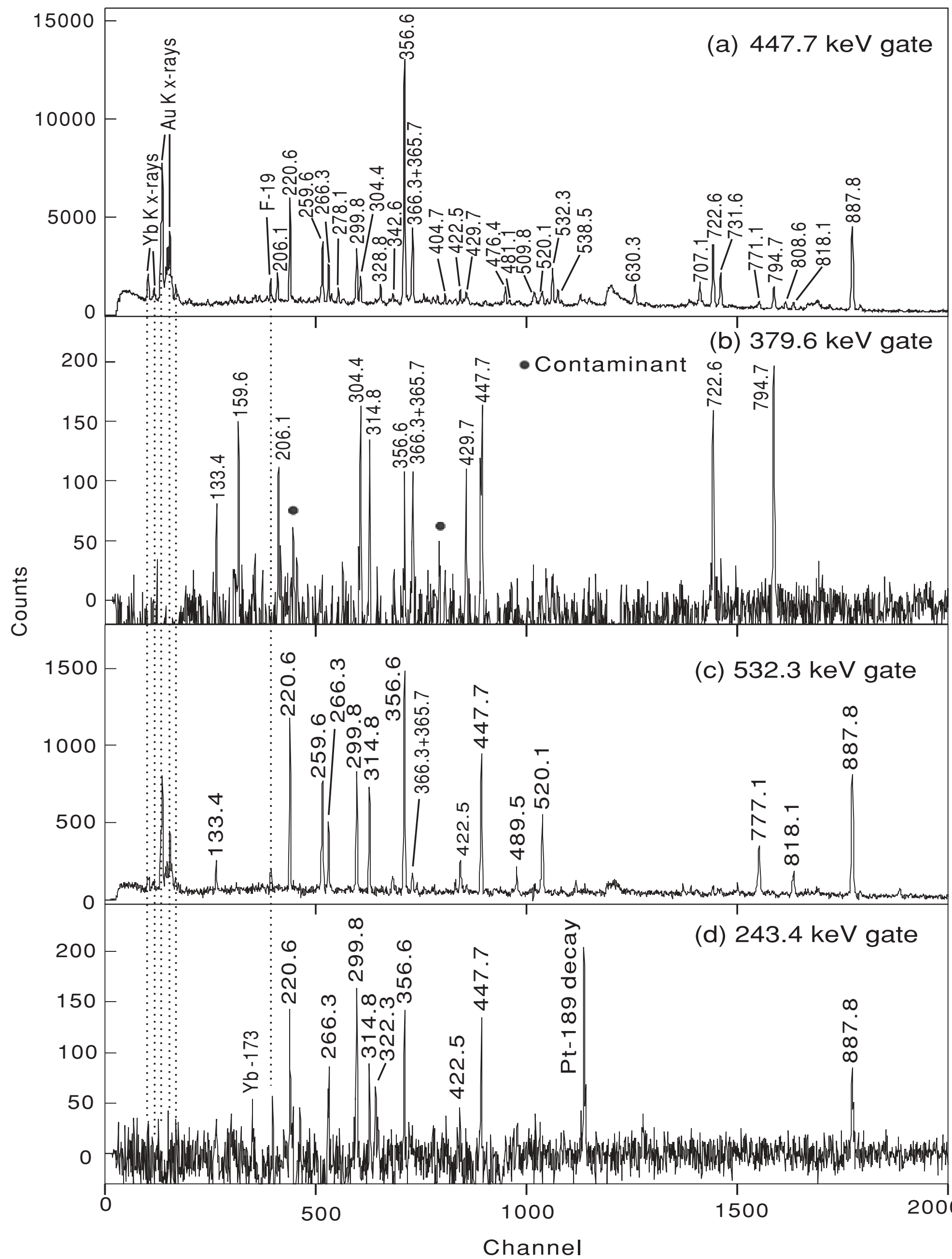

FIG. 3. Selected coincidence spectra for bands (a) and (b) and structure (c).

(ii) From the 597.3-keV gated spectrum [see Fig. 4(b)], the intensity of 337.7-keV transition is deduced to be ~70% of the intensity of the 493.1-keV transition. Considering the the intensity balance, the rest of the total intensity (~30%) is attributable to the 65.4- and 272.4-keV cascade transitions, as shown in Fig. 2. This assignment is supported by the 370.3-keV gated spectrum [see Fig. 4(c)], in which the intensity ratio $I_\gamma(272.4\,\mathrm{keV})/I_\gamma(377.7\,\mathrm{keV}) = 0.31(4)$ is obtained.

(iii) The γ-γ coincidence relationships and γ-ray energy sums of band (d) confirm the 273.1-keV transition in band (d). This is further supported by the 337.7-keV gated spectrum as only a 273.1-keV peak has been observed.

In addition to band (d), another weakly populated band [labeled as band (e) in Fig. 2] has been identified and assigned to ^{188}Au. A typical coincidence spectrum gated on the 328.3-keV line is presented in Fig. 6, where most of the γ rays in band (e) can be seen. The γ rays assigned to band (e) are in coincidence with the Au K x rays. From detailed analysis on the γ-γ coincidence relationships, five crossover transitions have been found for each sequence of band (e). The order of transitions was fixed with the observation of in-band transitions.

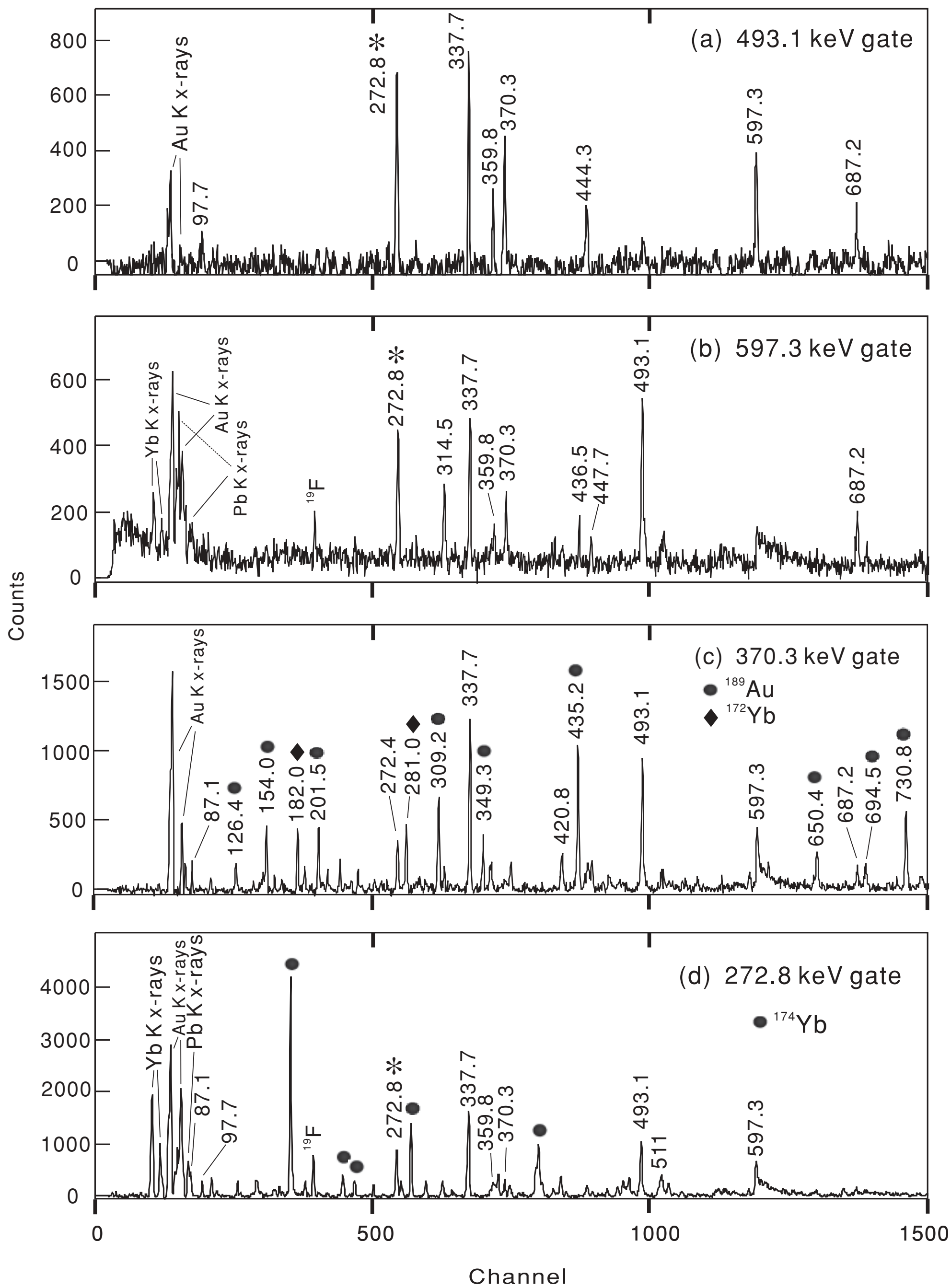

FIG. 4. γ-ray spectra gated by the (a) 493.1-keV transition, (b) 597.3-keV transition, (c) 370.3-keV transition, and (d) 272.8-keV transition. Lines marked with an asterisk are doublets.

III. DISCUSSION

A. Theoretical calculations

To investigate the shapes associated with the bands observed in our experiment, we have performed CSM calculations by means of TRS method [16] in the three-dimensional deformation β_2, β_4, and γ space. The nonaxial deformed Woods-Saxon (WS) potential [17] was employed. Both monopole and quadrupole pairings [18,19] were included. To avoid the spurious pairing phase transition encountered in the BCS approach, we used the approximate particle number projection named the Lipkin-Nogami pairing [20]. The pairing correlation is dependent on rotational frequency ($\hbar\omega$) and deformation. To include such dependence in the TRS calculations, we have done pairing-deformation-frequency self-consistent TRS calculations; that is, for any given frequency and deformation, the pairing is self-consistently calculated by the HFB-like method [20]. At a given frequency, the deformation of a state is determined by minimizing the calculated TRS.

TRSs were calculated for the four lowest-lying configurations of each parity and signature combination. The variation

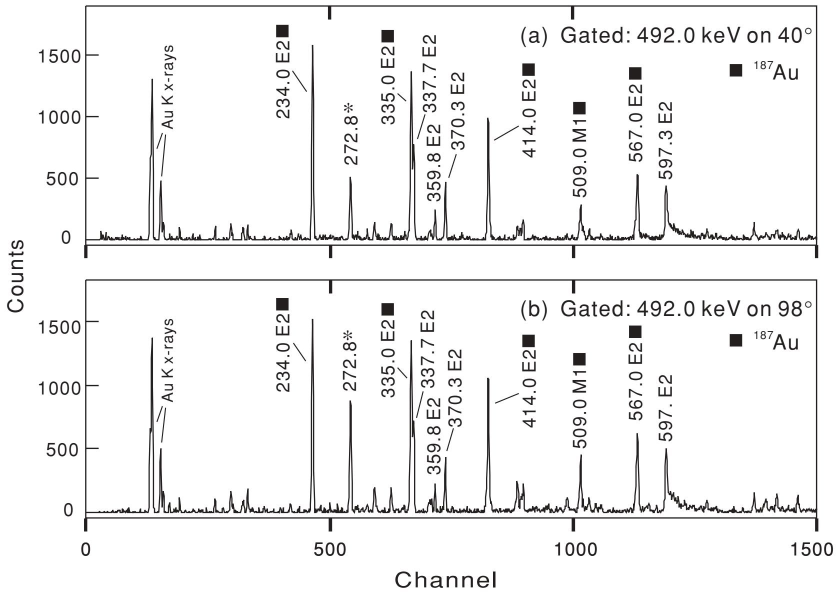

FIG. 5. Projected spectra at 40° (top panel) and 98° (bottom panel) gated by the 492.0-keV transition at all angles. Lines marked with an asterisk are doublets.

of the shape parameters as a function of rotational frequency has been examined for these configurations. Figure 7 shows the calculated energy surfaces for selected multiquasiparticle configurations in ^{188}Au and ^{186}Au. Axially symmetric prolate shapes correspond to $\gamma = 0^\circ$ and axially symmetric oblate shapes have $\gamma = -60^\circ$ for collective rotation. The parameters of the equilibrium shapes from TRS calculations corresponding to those selected configurations are summarized in Table II. TRS plots for single quasiproton and quasineutron configurations at low rotational frequencies in ^{191}Au and ^{190}Au, respectively, are published in Ref. [11]. From our calculations combined with the results of Ref. [11], the following interesting features emerge: (i) The energy surfaces have soft minima with respect to the deformation parameter γ. (ii) Calculations for configurations containing quasiprotons show large triaxiality partly owing to the involvement of an e $(-, -1/2)$ Routhian derived from the $\pi h_{11/2}$ subshell, which drives the shape toward $\gamma \sim -80^\circ$ (see also in Ref. [11]). (iii) The calculations predict that the quadrupole deformation decreases with increasing neutron number for the odd-odd-mass ^{186,188}Au nuclei in the $\pi h_{9/2} \bigotimes \nu i_{13/2}$ configuration, while the triaxiality parameter changes from $\gamma \approx 12^\circ$ to $\gamma \approx -33^\circ$. This indicates that a triaxial shape transition from prolate to oblate shape may take place in this region. (iv) The quadrupole deformation for the $\pi(-\frac{1}{2}, +\frac{1}{2}) \bigotimes \nu(-\frac{1}{2}, +\frac{1}{2})$ configuration, $\beta_2 \approx 0.206$, is slightly higher than those of other configurations in ^{188}Au, while the triaxiality parameter is $\gamma \approx 17^\circ$, indicating a near prolate shape for this configuration. The TRS calculations thus predict nonaxial shape for several configurations in ^{188}Au. These shape variations are expected to influence the nuclear properties, such as the relative position of the orbitals and their slopes, signature splitting, and signature crossing frequencies [21]. To study the possible influence of such nonaxial shape on nuclear properties, CSM calculations are then performed with a universal WS potential for ^{188}Au using $\beta_2 \approx 0.16$, $\beta_4 \approx -0.027$, as obtained from the TRS calculations, and for deformations of $\gamma = -30^\circ, -60^\circ, -70^\circ$, and -80°. The results for neutron quasiparticle Routhians are shown in Fig. 8, from which a strong dependence on γ deformation can be seen for the positive-parity A, B, and C Routhians (originating from low-K $\nu i_{13/2}$ orbitals). As γ decreases from -30° toward -80° the B Routhian drops down, while the A Routhian rises, which leads to a decrease of the signature splitting and to a signature inversion for $\gamma \leqslant -70^\circ$. We notice that the F Routhian drops down very fast for larger nonaxiallity. The results of the TRS and CSM calculations are used to discuss the observed structures in ^{188}Au.

B. Band structure

The absolute excitation energies of new bands (d) and (e) presented in Fig. 2 are not known because neither interband

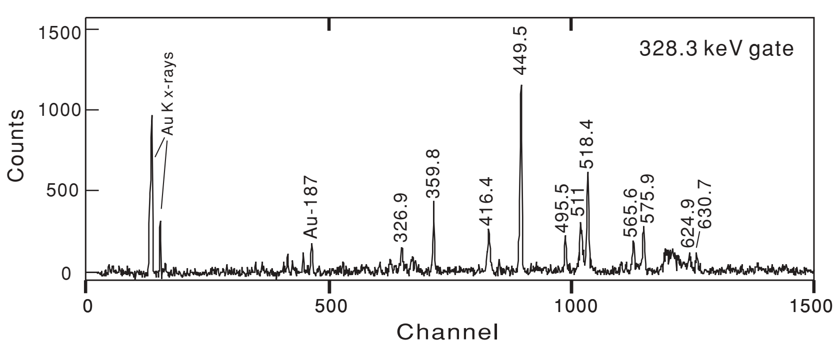

FIG. 6. The γ-ray spectra gated by the 328.3-keV transition.

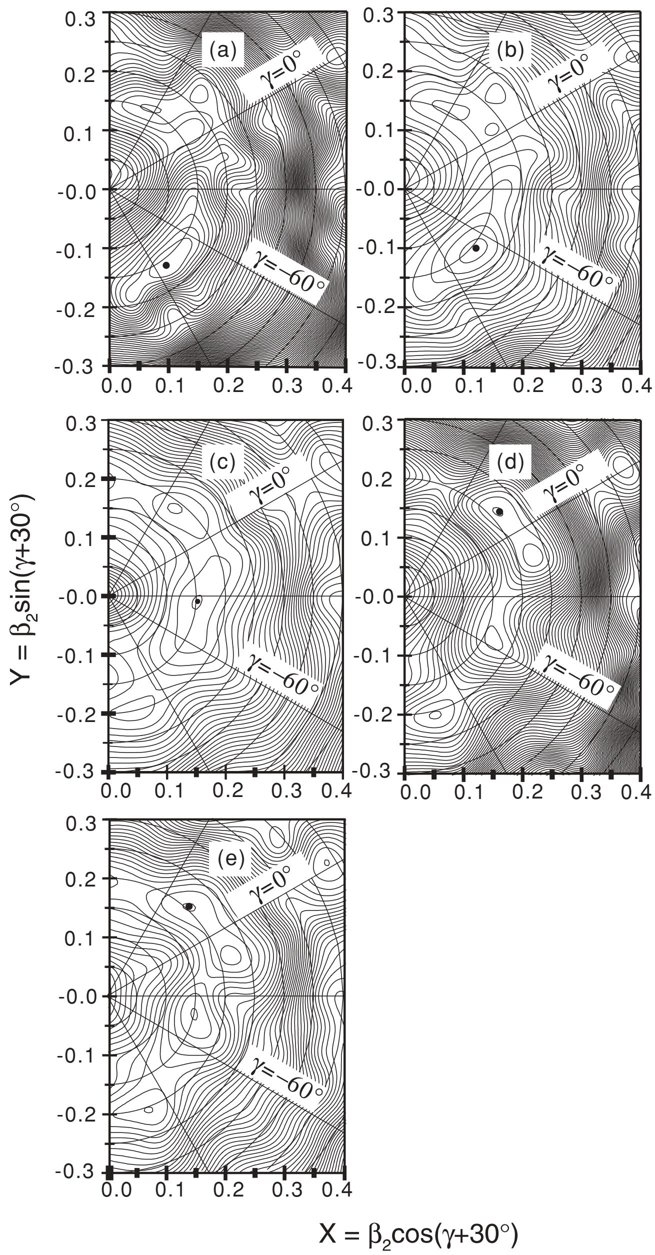

FIG. 7. TRS calculations for selected configurations. (a) 11^- sequence of band (a) in ^{188}Au, calculated at $\hbar\omega = 0.20$ MeV; (b) 12^- sequence of band (a) in ^{188}Au, calculated at $\hbar\omega = 0.20$ MeV; (c) favored sequence of band (e) in ^{188}Au, calculated at $\hbar\omega = 0.16$ MeV; (d) favored sequence of $\pi h_{9/2} \otimes \nu i_{13/2}$ band in ^{186}Au, calculated at $\hbar\omega = 0.16$ MeV; (e) $\pi(-\frac{1}{2}, +\frac{1}{2}) \otimes \nu(-\frac{1}{2}, +\frac{1}{2})$ configuration in ^{188}Au, calculated at $\hbar\omega = 0.18$ MeV.

connections nor connections from these bands to the known states or ground states could be established. Because no firm spin and parity assignments can be made in the present work, our discussion is therefore based on systematics and theoretical arguments. Our TRS calculations for ^{188}Au predict $|\beta_2| \approx 0.16$ and 0.22 for nearly oblate and prolate deformations, respectively. The orbitals closest to the Fermi level for these deformations are low-Ω orbitals from $\nu i_{13/2}$ and $\nu h_{9/2}$ shells, low-j orbitals from $\nu p_{3/2}$ and $\nu f_{5/2}$ shells, as well as low-Ω orbitals from $\pi h_{11/2}$ and $\pi h_{9/2}$. Experimentally, in the neighboring odd-Z ^{187,189}Au [8,9] nuclei, the oblate ground state based on the low-Ω $\pi h_{11/2}$ configuration is found. However, prolate structure based on the low-Ω $\pi h_{9/2}$ configuration is also observed. As for the nearby odd-N ^{187}Pt [22], ^{189}Hg [23], and ^{185}Os [24] nuclei, the $\nu i_{13/2}$, $\nu f_{5/2}$, and $\nu p_{3/2}$ configurations are populated in heavy-ion-induced fusion-evaporation reactions. Thus, combinations of these protons and neutrons orbitals are primarily considered for the configurations of the bands in ^{188}Au.

TABLE II. Calculated equilibrium deformations β_2 and γ from the TRS calculations for selected configurations in ^{188}Au and ^{186}Au at relevant rotational frequencies $\hbar\omega$.

Nucleus	Configuration	α	$\hbar\omega$	β_2	γ
^{188}Au	$\pi h_{11/2}^{-1} \otimes \nu i_{13/2}^{-1}$	0	0.20	0.157	−69
^{188}Au	$\pi h_{11/2}^{-1} \otimes \nu i_{13/2}^{-1}$	1	0.20	0.161	−83
^{188}Au	$\pi h_{9/2} \otimes \nu i_{13/2}$	0	0.16	0.153	−33
^{186}Au	$\pi h_{9/2} \otimes \nu i_{13/2}$	0	0.16	0.216	12
^{188}Au	$\pi(-\frac{1}{2}, +\frac{1}{2}) \otimes \nu(-\frac{1}{2}, +\frac{1}{2})$	1	0.18	0.206	17

1. *Bands (a) and (b) and structure (c)*

Band (a) was previously assigned to be built on an oblate $\pi h_{11/2}^{-1} \otimes \nu i_{13/2}^{-1}$ configuration [7]. (Note that we write $\pi^- \otimes \nu^-$ for hole configurations and $\pi \otimes \nu$ for particle configurations.) The experimental Routhians of band (a) in ^{188}Au are shown in the top panel of Fig. 9. We used the same Harris parameters of $J_0 = 7\hbar^2$ MeV^{-1} and $J_1 = 40\hbar^4$ MeV^{-3} as those in Ref. [7]. It is clearly shown in this figure that the signature inversion in the $\pi h_{11/2}^{-1} \otimes \nu i_{13/2}^{-1}$ band has been observed below $\hbar\omega = 0.35$ MeV, above which the signature splitting becomes normal. This frequency is usually called the signature crossing frequency. The signature inversion appears in the $\pi h_{11/2}^{-1} \otimes \nu i_{13/2}^{-1}$ band in the doubly odd $^{186-194}$Au nuclei [7,25,26]. This phenomenon is manifested by the inverted position of the experimental Routhians at low rotational frequency; that is, the Routhian of the unfavored signature (11^- sequence) lies lower than the Routhian of the favored signature (12^- sequence), while the normal position is restored at higher rotational frequency. Theoretical calculations within the framework of the CSM for ^{186,188}Au nuclei predicted a signature crossing at 0.22 MeV if a nonaxial shape with $\gamma \sim -70^\circ$ is assumed [7]. These results have been confirmed in our calculations. As shown in the bottom panel of Fig. 8, the B Routhians become yrast at low rotational frequency for $\gamma \leqslant -70^\circ$. In fact, the TRS calculations predict nonaxial deformation of $\beta_2 = 0.161$, $\gamma \sim -83^\circ$ for the unfavored signature and $\beta_2 = 0.157$, $\gamma \sim -69^\circ$ for the favored signature (see Table II). To fully understand the experimental signature crossing frequency, the CSM Routhians for the unfavored and favored signatures in ^{188}Au are constructed using the sum of the e and B (using the CSM labels) diabatic Routhians calculated at $\gamma = -80^\circ$ and the sum of the e and A Routhians calculated at $\gamma = -70^\circ$, respectively. The results are shown in the bottom panel of Fig. 9; the experimental signature inversion can be well reproduced by the calculations. In particular, the theoretical

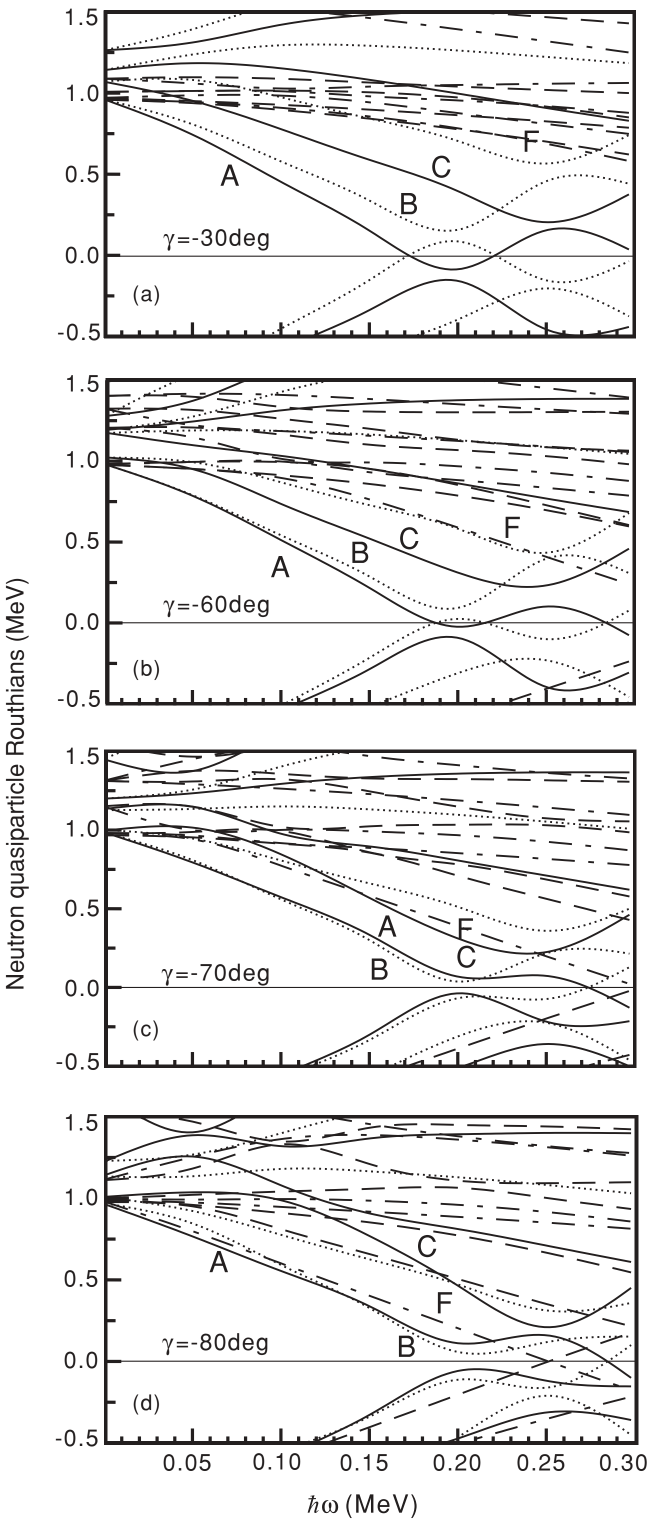

FIG. 8. Cranked-shell-model calculations for neutrons in ^{188}Au. The Woods-Saxon potential with universal parameters is used. Deformation parameters of $\beta_2 = 0.16$, $\beta_4 = -0.027$ are chosen. The Routhian with $(\pi, \alpha) = (+, +1/2)$ are drawn with a solid line, $(+, -1/2)$ with a dotted line, $(-, +1/2)$ with a dash-dotted line, and $(-, -1/2)$ with a dashed line.

signature crossing frequency of 0.36 MeV is in excellent agreement with the experimentally measured one of 0.35 MeV.

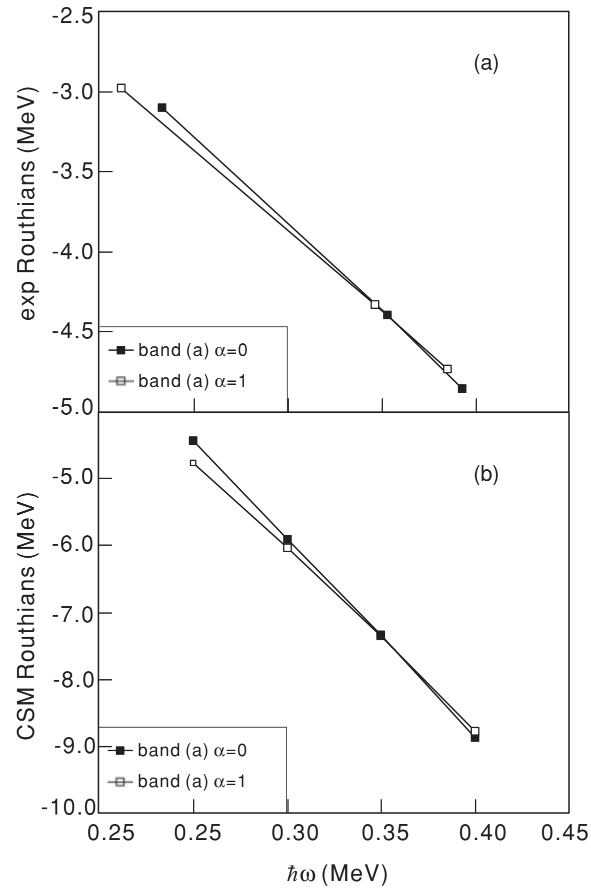

FIG. 9. Experimental Routhians (top panel) for the band (a) in ^{188}Au. The Harris reference parameters are chosen to be $J_0 = 7\hbar^2\ \mathrm{MeV}^{-1}$ and $J_1 = 40\hbar^4\ \mathrm{MeV}^{-3}$. The CSM Routhians (bottom panel) for the unfavored signature and favored signature were calculated for the predicted γ deformations of -80° and -70°, respectively.

It is worth noting that a strong 630.3- to 707.1-keV sequence, $(20^-)\rightarrow(18^-)\rightarrow(16^-)$, can be seen in Fig. 2. This sequence has a close relationship with the *eA* and *eB* configurations of band (a) and might be the third signature $\alpha = 0$ with *eC* configuration. This assignment is supported by the TRS and CSM calculations. One can see in Fig. 8, the *C* Routhian drops down and lies close in energy with *A* and *B* Routhians if a nonaxial shape with $\gamma \leqslant -70^\circ$ is assumed. The nonaxiality is induced by the odd $\pi h_{11/2}$ proton, as predicted by the TRS calculation.

The 532-777-818-keV cascade of band (b) was placed directly on top of the (18^+) level by Janzen *et al.* [7], suggesting that this cascade belongs to the structure built on the (15^+) levels. This (15^+) state was considered as the onsets of semidecoupled bands with a $\pi h_{11/2}^{-1} \otimes \nu i_{13/2}^{-2} j$ [$j = (p_{3/2}, f_{5/2})$] four-quasiparticle configuration [7]. It has been pointed out [7] that some changes in the intrinsic structure may take place at spins around $18\hbar$. With the newly observed 18^+ level, we were able to identity two different structures built on top of the new $I^\pi = 20^+$ and $I^\pi = 15^+$ levels, corresponding to band (b) and structure (c), respectively. Band (b) should be based on the $\pi h_{11/2}^{-1} \otimes \nu i_{13/2}^{-2} h_{9/2}^{-1}$ configuration.

This assignment is suggested according to the following considerations: (i) The excitation energy of the $I^\pi = 20^+$ level in the ^{188}Au nucleus relative to the $I^\pi = 11^-$ level $(\pi h_{11/2}^{-1} \otimes \nu i_{13/2}^{-1})$ corresponds to a two-quasiparticle excitation. Therefore, the $I^\pi = 20^+$ level should be associated with a four-quasiparticle state. Considering the orbitals closest to the Fermi level, the 20^+ state should be constructed most probably by the excitation of $\pi h_{11/2}^{-1} \otimes \nu i_{13/2}^{-2} h_{9/2}^{-1}$ or $\pi h_{11/2}^{-1} \otimes \nu i_{13/2}^{-2} f_{7/2}^{-1}$ configurations. The total aligned spin of the $\pi h_{11/2}^{-1} \otimes \nu i_{13/2}^{-2} h_{9/2}^{-1}$ and $\pi h_{11/2}^{-1} \otimes \nu i_{13/2}^{-2} f_{7/2}^{-1}$ configurations would result in $I^\pi = 22^+$ and $I^\pi = 21^+$, respectively. However, the former configuration is still more likely, because the $\nu h_{9/2}$ shell lies closer to the Fermi level. (ii) The $I^\pi = 20^+$ level has been identified to be isomeric in ^{190,192}Au and the $\pi h_{11/2}^{-1} \otimes \nu i_{13/2}^{-2} h_{9/2}^{-1}$ configuration is proposed for this level [12]. Moreover, in the neighboring even-even ^{190,192}Pt and odd-even $^{187-193}$Au nuclei, the $\nu i_{13/2}^{-1} h_{9/2}^{-1}$ and the $\pi h_{11/2}^{-1} \otimes \nu i_{13/2}^{-1} h_{9/2}^{-1}$ configurations have been assigned to the $I^\pi = 10^-$ and $I^\pi = 13/2^+$ isomeric states, respectively, based on the g-factor measurements [27,28]. We noted that the half-life of the 20^+ state for ^{188}Au cannot be extracted in this experiment. (iii) The CSM calculations show that the F Routhian originating from the $\nu h_{9/2}$ subshell drops down and lies close in energy with A, B Routhians if a nonaxial shape with $\gamma \sim -80^\circ$ is assumed (see bottom panel of Fig. 8), leading to an easier observation of $\pi h_{11/2}^{-1} \otimes \nu i_{13/2}^{-2} h_{9/2}^{-1}$ band in our experiment.

The (15^+) level has been proposed [7] to be the onset of the semidecoupled band [labeled (c)] in ^{188}Au and assigned to the $\pi h_{11/2}^{-1} \otimes \nu i_{13/2}^{-2} j$ $[j = (p_{3/2}, f_{5/2})]$ configuration. The level structures associated with $\pi h_{11/2}^{-1} \otimes \nu i_{13/2}^{-2} j$ $[j = (p_{3/2}, f_{5/2})]$ configuration were observed in odd-odd $^{186-194}$Au nuclei [7,25,26]. It has been characterized as $\pi h_{11/2}^{-1} \otimes \nu i_{13/2}^{-1}$ excitations coupled to the known (5^-) state in the oblate Hg core nuclei. In the Au isotopes these bands are weakly populated with respect to those in the Hg and Pt isotopes using heavy-ion-induced fusion-evaporation reactions. As proposed by Gueorguieva *et al.* [10], such a difference in the population pattern is most likely attributable to the deformation driving properties of the odd $h_{11/2}$ proton, which induces nonaxial shapes in the Au isotopes, and causes the $\nu h_{9/2}$ orbitals to drop much closer to the Fermi level. Thus, the energy levels involving such orbitals [like the levels above the (20^+) and (23^-) states in the odd-odd and above the $(31/2^+)$ and $(39/2^-)$ states in the odd-even Au isotopes] become yrast. The same explanation could be applied to ^{188}Au.

2. *Band (d)*

A large signature splitting has been observed in band (d), indicating that the low-Ω quasiproton and quasineutron are likely involved in its configuration. Candidate configurations are $\pi h_{9/2} \otimes (\nu f_{5/2}, \nu p_{3/2})$ and $\pi h_{11/2}^{-1} \otimes \nu h_{9/2}^{-1}$, corresponding to prolate and oblate deformations, respectively. We noticed that no analogous structure has been observed so far in the odd-odd Au nuclei.

The level structure in band (d) is compared in Fig. 10 with the doubly decoupled band in ^{186}Ir [29] along with the ground state band of ^{184}Os [30]. The similarity of transition energies is clearly seen among the three bands with the exception of two low-lying transitions. This resemblance can be explained by decoupling the odd quasiproton and quasineutron of ^{188}Au and ^{186}Ir from the prolate ^{184}Os core. Moreover, the differences in consecutive transition energies between the bands of ^{188}Au and ^{186}Ir, $\triangle E_\gamma$, is about 22 keV, indicating the nearly identical dynamic moment of inertia (MOI) defined as $dI/d\omega = \triangle I/\triangle\omega = 4/\triangle E_\gamma$. The doubly decoupled band in ^{186}Ir was proposed to be a pseudospin doublet structure of $1/2[541] \otimes [\widetilde{411}, \pm 1/2]$ configuration, corresponding to the Nilsson orbitals labeled conventionally as 3/2[512] and 1/2[510] [29]. It seems reasonable to assign the similar quasiparticle configuration to band (d) in ^{188}Au. This assignment is further supported by the TRS calculations as a near prolate deformation has been predicted for the $\pi(-\frac{1}{2}, +\frac{1}{2}) \otimes \nu(-\frac{1}{2}, \pm\frac{1}{2})$ configuration [see Fig. 7(e)].

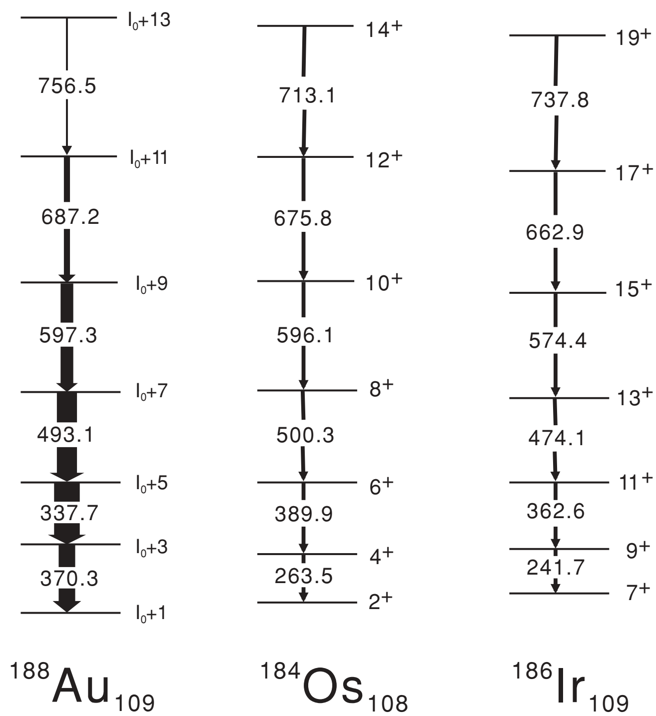

FIG. 10. Comparison of ground-state band in the even-even ^{184}Os [30] and the favored members of the $1/2[541] \otimes [\widetilde{411}, \pm 1/2]$ band in ^{186}Ir [29] with the favored members of band (d) in ^{188}Au.

A different interpretation, that band (d) is a hole in the low-Ω $\pi h_{11/2}$ and $\nu h_{9/2}$ shells coupling to the oblate Hg core, is likely because the oblate deformation is predicted to dominate for $A \geqslant 187$ Au isotopes. This assignment is consistent with the fact that band (d) is populated more stronger than band (e) $(\pi h_{9/2} \otimes \nu i_{13/2})$. Indeed, the CSM calculations, as already discussed, predict that the F Routhian originating from the $\nu h_{9/2}$ subshell drops down and lies close in energy with A, B Routhians owing to the nonaxiallity of nuclear shape in ^{188}Au (see Fig. 8).

However, because the spin and parity assignments of band (d) are not clear at this time, it is hard to give preference to

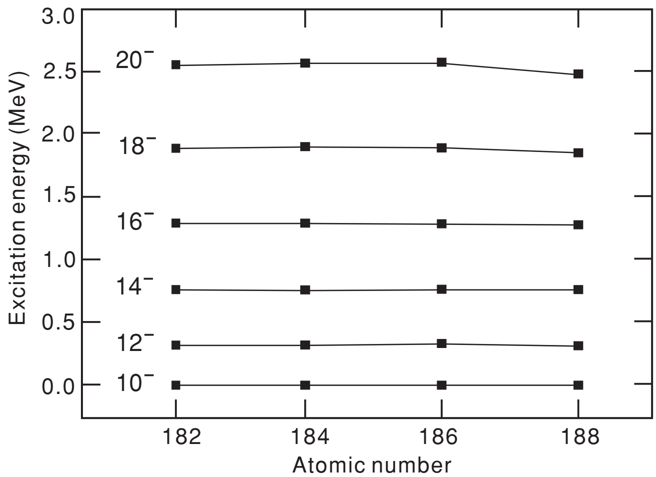

FIG. 11. Experimental excitation energies of the unfavored members of the $\pi h_{9/2} \otimes \nu i_{13/2}$ band relative to (10^-) state in the odd-odd Au isotopes ^{182}Au [32], ^{184}Au [4], ^{186}Au [7], and ^{188}Au (this work). The bandhead spin and parity of (10^-) is accepted for band (e) in ^{188}Au.

one of the preceding possibilities. It is worth noting that band (d) does not form a well-defined rotational pattern; that is, the low-lying $E2$ transition energies vary in an irregular manner with spin (regular bands should have transition energies which increase smoothly with spin). We cannot give a detailed explanation for the mechanism leading to these irregular $E2$ transitions, but we suggest that band (d) might be associated with configurations for which the potential energy surface is soft in the γ degree of freedom or that the low-lying states might have a different configuration from the higher-spin states of band (d). Clearly, more data and calculations are needed to solve this problem.

3. *Band (e)*

The irregular $\Delta I = 1$ transition energies in band (e) present a common feature of semidecoupled band in odd-odd nuclei [31]. For such a semidecoupled two-quasiparticle band, one quasiarticle occupies only the signature-favored state of an $\Omega = 1/2$ orbital. Another quasiparticle locates at the middle of a high-j shell and can occupy signature-favored and unfavored levels owing to its small signature splitting. With this information, band (e) should be based on $\pi h_{9/2}(1/2^-[541]) \otimes \nu i_{13/2}$ configuration. It is worth noting that the bands built on the same configuration have been observed in ^{182,184,186}Au [4,7,32]. The excitation-energy systematics for the unfavored (signature $\alpha = 0$) $\Delta I = 2$ transition sequences in the $\pi h_{9/2} \otimes \nu i_{13/2}$ bands of odd-odd Au isotopes are shown in Fig. 11, where the energies are given relative to the assigned (10^-) state for each isotope. As is clear from this figure, the level energies of these bands exhibit smooth trends for Au isotopes. The level energies of band (e) in ^{188}Au fit well with the systematics if the proposed I^π values are accepted.

The band (e) displays very large signature splitting (originating from $\nu i_{13/2}$ orbital) at low rotational frequency. The signature splitting Δe is defined as the difference in energies at a given rotational frequency for the pair of signature partners. Figure 12 presents plots of the signature splitting for the $\pi h_{9/2} \otimes \nu i_{13/2}$ bands in odd-odd $^{182-188}$Au [4,7,32], defined as $S(I) = [E(I) - E(I-1)] - 1/2[E(I+1) - E(I) + E(I-1) - E(I-2)]$. Here $E(I)$ is the level energy of state I; $S(I)$ is directly proportional to the signature splitting Δe, but magnified by approximately a factor of 2. As shown in Fig. 12, the amplitude of signature splitting in ^{188}Au is larger than those of odd-odd $^{182-186}$Au, and it decreases with the increasing rotational frequency. The signature splitting can be interpreted as arising from mixing of an $\Omega = 1/2$ component into the high-K $\nu i_{13/2}$ neutron configuration. However, because the neutron Fermi level is situated high in the $\nu i_{13/2}$ subshell in ^{188}Au with a neutron number of 109, the normal Coriolis mixing of the $\Omega = 1/2$ component into the wave function is expected to be low for an axially symmetric nucleus. Therefore, to reproduce the large signature splitting observed in the $\pi h_{9/2} \otimes \nu i_{13/2}$ band, a mechanism leading to enhanced mixing with an $\Omega = 1/2$ orbit is needed. This can be achieved by a departure from an axially symmetric shape for which K is no longer a good quantum number. We have noticed that large signature splittings have also been observed in the $\nu i_{13/2}$ bands in the isotone ^{187}Pt [22] and lighter odd-A Pt nuclei [33–35]. These large signature splittings have been attributed to the triaxial shape and the negative values of β_4 [34,35]. The same explanation could be applied to ^{188}Au.

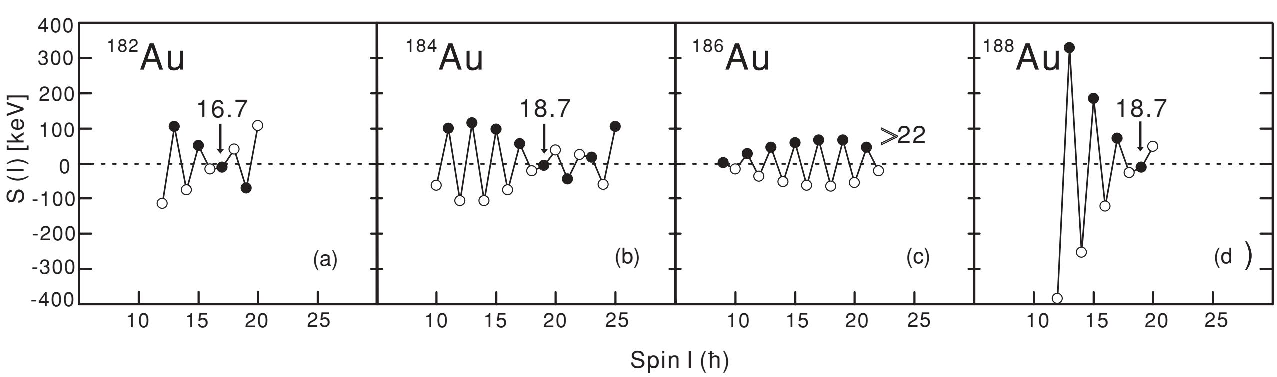

FIG. 12. Plot of signature splittings $S(I)$ vs I for the $\pi h_{9/2} \otimes \nu i_{13/2}$ bands observed in ^{188}Au and the corresponding bands in ^{182}Au [32], ^{184}Au [4], and ^{186}Au [7]. The solid (open) symbols correspond to the signature favored (signature unfavored) levels. The arrows indicate the signature crossing spins.

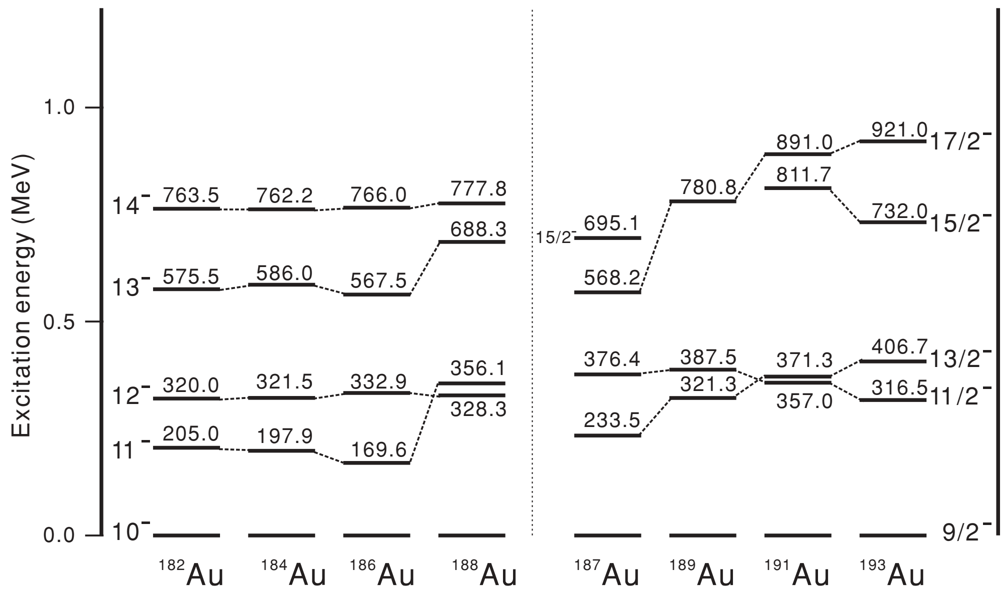

FIG. 13. Partial levels in the $\pi h_{9/2} \otimes \nu i_{13/2}$ bands for the odd-odd nuclei ^{182}Au [32], ^{184}Au [4], ^{186}Au [7], and ^{188}Au (this work) and $\pi h_{9/2}$ bands for the odd-A ^{187}Au [8], ^{189}Au [9], and ^{191,193}Au [13].

One can see in Fig. 12 that the points (associated with levels $I's$) that have negative values are energetically favored over those with positive ones. The expected favored signature is $\alpha_f = 1$ for the $\pi h_{9/2} \otimes \nu i_{13/2}$ configuration. It can be seen in this figure that at low spins, it is the $\alpha_{uf} = 0$ signature that is favored energetically rather than the $\alpha_f = 1$ sequence. Such behavior has been referred to as signature inversion or anomalous signature splitting [36]. With increasing angular momentum, the inverted signature splitting becomes decreasing, and the two signature branches cross with each other at certain spin I_c. Systematic studies and analyses have been made in Ref. [21] for the $\pi h_{9/2} \otimes \nu i_{13/2}$ configurations. A conclusion has been made that the signature crossing spin I_c increasing 2–3$\hbar$ with increasing two neutrons for the chain of isotopes. In view of Fig. 12, the signature crossing spin I_c is consistent with the systematic trends for ^{182,184,186}Au while it is not true for ^{188}Au. It has been suggested that the γ deformation and the residual interaction between high-j particles are the most important factors for the signature inversion [36,37]. Our TRS calculations for the $\pi h_{9/2} \otimes \nu i_{13/2}$ bands show a larger γ deformation and smaller β_2 in ^{188}Au than those of in ^{186}Au. This might explain the irregular change of the signature crossing spin I_c for the chain of Au isotopes.

Finally, we note that the (11^-) level in this band was observed at slightly higher excitation energy than the (12^-) level in ^{188}Au, while for ^{182,184,186}Au the favored member lies lower than the unfavored member (see the left panel of Fig. 13). In comparison, experimental data for the $\pi h_{9/2}$ bands in odd-mass $^{187-193}$Au nuclei are presented in the right panel of Fig. 13. It can be seen in this figure that in ^{187}Au, it is the favored members (e.g., $13/2^-$, $17/2^-$) that are favored energetically than the unfavored members (e.g., $11/2^-$, $15/2^-$), while for ^{193}Au this order is reversed. The transition takes place between ^{189}Au and ^{191}Au. This phenomenon in odd-mass $^{187-193}$Au has been interpreted, within the framework of the particle-plus-triaxial-rotor (PTR) model [13,38], as owing to a transition from prolate to oblate shape through $\gamma = 30^\circ$ (^{189}Au) occurring between ^{187}Au ($\gamma = 12^\circ$) and ^{193}Au ($\gamma = 58^\circ$). The $\pi h_{9/2} \otimes \nu i_{13/2}$ configuration cannot be found in the heavier odd-odd Au isotopes. This prevents us from making detailed discussion. Our TRS calculations predicted that in ^{188}Au there are two γ-soft minima, $\gamma = 19^\circ$ and $\gamma = -33^\circ$, with the $\gamma = -33^\circ$ minimum being slightly deeper, whereas for ^{186}Au the $\gamma = 12^\circ$ minimum is more favored (see Table II and Fig. 7). The ^{188}Au nucleus with $\gamma \sim -30^\circ$ is predicted to lie at the critical point of prolate-to-oblate shape transition. Thus, such an anomalous level behavior in ^{188}Au may be attributable to the change of nuclear shape. This shape variance of the $\pi h_{9/2} \otimes \nu i_{13/2}$ band in ^{188}Au probably reflects the position of neutron Fermi level in moving away from the neutron midshell ($N = 104$) owing to the decrease in the deformation and softness of γ degree of freedom.

IV. SUMMARY

In summary, we have studied the high-spin structure of ^{188}Au and extended the level scheme considerably compared to the previous studies. A new $I^\pi = 20^+$ state associated with $\pi h_{11/2}^{-1} \otimes \nu i_{13/2}^{-2} h_{9/2}^{-1}$ configuration and two new rotational bands, one of which is built on the $\pi h_{9/2} \otimes \nu i_{13/2}$ configuration, have been identified. These configurations were studied using TRS and CSM calculations. The calculations predicted that the low-Ω $\pi h_{11/2}$ orbitals induce a nonaxial shape with $\gamma < -70^\circ$. The experimental signature crossing frequency in the $\pi h_{11/2}^{-1} \otimes \nu i_{13/2}^{-1}$ band is quite well reproduced by the calculations using the nonaxial shape with $\gamma < -70^\circ$. The calculations predict that the quadrupole deformation of $\pi h_{9/2} \otimes \nu i_{13/2}$ bands decreases from ^{186}Au to ^{188}Au, while the triaxiality parameter changes from $\gamma \approx 12^\circ$ to $\gamma \approx -33^\circ$, indicating that a triaxial shape transition from prolate to oblate shape should occur around ^{188}Au. This prediction is in agreement with the experimental large signature splitting, the observed irregular signature crossing spin I_c and the anomalous level behavior in the $\pi h_{9/2} \otimes \nu i_{13/2}$ band in ^{188}Au.

ACKNOWLEDGMENTS

The research was performed with the JAEA Common Use Facility Program. The authors thank the staff at the JAEA tandem accelerator for providing the ^{19}F beam. This work was supported by the National Natural Sciences Foundation (Grants No. 10905075, No. 10825522, No. 10735010, and No. 10775158), the Major State Basic Research Development Program of China (Grant No. 2007CB815005), and the Chinese Academy of Sciences.

[1] S. Sakakihara and Y. Tanaka, Nucl. Phys. A **726**, 37 (2003).
[2] I. O. Morales, A. Frank, C. E. Vargas, and P. VanIsacker, Phys. Rev. C **78**, 024303 (2008).
[3] P. M. Davidson, G. D. Dracoulis, T. Kibédi, A. P. Byrne, S. S. Anderssen, A. M. Baxter, B. Fabricius, G. J. Lane, and A. E. Stuchbery, Nucl. Phys. A **657**, 219 (1999), and references therein.
[4] F. Ibrahim *et al.*, Phys. Rev. C **53**, 1547 (1996).
[5] Y. H. Zhang *et al.*, Chin. Phys. Lett. **21**, 799 (2004).
[6] P. Joshi, A. Kumar, I. M. Govil, R. P. Singh, G. Mukherjee, S. Muralithar, R. K. Bhowmik, and U. Garg, Phys. Rev. C **69**, 044304 (2004).
[7] V. P. Janzen *et al.*, Phys. Rev. C **45**, 613 (1992).
[8] J. K. Johansson, D. G. Popescu, D. D. Rajnauth, J. C. Waddington, M. P. Carpenter, L. H. Courtney, V. P. Janzen, A. J. Larabee, Z. M. Liu, and L. L. Riedinger, Phys. Rev. C **40**, 132 (1989).
[9] N. Perrin, A. Korichi, C. Bourgeois, F. Azaiez, J. Duprat, F. Ibrahim, D. Hojman, F. Le Blanc, D. G. Popescu, and H. Sergolle, Z. Phys. A **347**, 81 (1993).
[10] E. Gueorguieva, C. Schuck, A. Minkova, Ch. Vieu, M. Kaci, F. Hannachi, R. Wyss, J. S. Dionisio, A. Korichi, and A. Lopez-Martens, Phys. Rev. C **69**, 044320 (2004).
[11] E. Gueorguieva *et al.*, Phys. Rev. C **68**, 054308 (2003).
[12] E. Gueorguieva *et al.*, Phys. Rev. C **64**, 064304 (2001).
[13] Y. Oktem *et al.*, Phys. Rev. C **76**, 044315 (2007).
[14] K. Furuno *et al.*, Nucl. Instrum. Methods A **421**, 211 (1999).
[15] M. C. Abreu, V. Berg, K. Fransson, A. Höglund, J. Oms, and M. G. Porquet (The Isocele Collaboration), Nucl. Phys. A **437**, 324 (1985).
[16] W. Nazarewicz, R. Wyss, and A. Johnson, Phys. Lett. B **225**, 208 (1989).
[17] W. Nazarewicz, J. Dudek, R. Bengtsson, and I. Ragnarsson, Nucl. Phys. A **435**, 397 (1985).
[18] W. Satula and R. Wyss, Phys. Rev. C **50**, 2888 (1994).
[19] F. R. Xu, W. Satula, and R. Wyss, Nucl. Phys. A **669**, 119 (2000).
[20] W. Satula, R. Wyss, and P. Magierski, Nucl. Phys. A **578**, 45 (1994).
[21] Y. H. Zhang *et al.*, Phys. Rev. C **68**, 054313 (2003), and references therein.
[22] X. H. Zhou *et al.*, Phys. Rev. C **75**, 034314 (2007).
[23] I. G. Bearden *et al.*, Nucl. Phys. A **576**, 441 (1994).
[24] T. Shizuma, S. Mitarai, G. Sletten, R. A. Bark, N. L. Gjorup, H. J. Jensen, M. Piiparinen, J. Wrzesinski, and Y. R. Shimizu, Phys. Rev. C **69**, 024305 (2004).
[25] A. Neskakis, R. M. Lieder, H. Beuscher, Y. Gono, D. R. Haenni, and M. Müller-Veggian, Nucl. Phys. A **390**, 53 (1982).
[26] A. Neskakis, R. M. Lieder, H. Beuscher, Y. Gono, D. R. Haenni, M. Müller-Veggian, and C. Mayer-Böricke, Phys. Lett. B **80**, 194 (1979).
[27] N. Perrin, C. Bourgeois, A. Korichi, M. Pautra, H. Sergolle, N. Barré, C. Vieu, N. Benouaret, and J. Vanhorenbeeck, Z. Phys. A **359**, 373 (1997).
[28] A. Levon *et al.*, *International Conference on Advances in Nuclear Physics* (Giahoudi-Giapouli Pub., Thessaloniki, 1997).
[29] M. A. Cardona *et al.*, Phys. Rev. C **55**, 144 (1997).
[30] C. Wheldon *et al.*, Nucl. Phys. A **699**, 415 (2002).
[31] A. J. Kreiner, J. Davidson, M. Davidson, D. Abriola, C. Pomar, and P. Thieberger, Phys. Rev. C **36**, 2309 (1987); **37**, 1338 (1988).
[32] Y. H. Zhang *et al.*, Eur. Phys. J. A **14**, 271 (2002).
[33] S. Pilotte, G. Kajrys, S. Monaro, M. P. Carpenter, V. P. Janzen, L. L. Riedinger, J. K. Johansson, D. G. Popescu, D. D. Rajnauth, and J. C. Waddington, Phys. Rev. C **40**, 610 (1989).
[34] J. Nyberg *et al.*, Nucl. Phys. A **511**, 92 (1990).
[35] M. J. A. De Voigt, R. Kaczarowski, H. J. Riezebos, R. F. Noorman, J. C. Bacelar, M. A. Deleplanque, R. M. Diamond, and F. S. Stephens, Nucl. Phys. A **507**, 447 (1990).
[36] R. Bengtsson, H. Frisk, R. F. May, and J. A. Pinston, Nucl. Phys. A **415**, 189 (1984).
[37] R. A. Bark *et al.*, Nucl. Phys. A **630**, 603 (1998), and references therein.
[38] Y. Gono, R. M. Lieder, M. Müller-, Veggian A. Neskakis, and C. Mayer-Böricke, Nucl. Phys. A **327**, 269 (1979).